

3D printing of curved concrete surfaces using Adaptable Membrane Formwork

Jian Hui Lim*, Yiwei Weng*, Quang-Cuong Pham*

Singapore Centre for 3D Printing, School of Mechanical & Aerospace Engineering, Nanyang Technological University, 50 Nanyang Avenue, 639798, Singapore



HIGHLIGHTS

- 3D printed a non-developable Dome and Saddle concrete panel.
- Proposed a method for the development of 3D printed curved concrete panels.
- Proposed a method to quantify the geometric fidelity of the printed panels.

ARTICLE INFO

Article history:

Received 10 April 2019

Received in revised form 20 September 2019

Accepted 24 September 2019

Available online 18 October 2019

Keywords:

3D concrete printing

Facade

Non-developable surfaces

Adaptable Membrane Formwork

ABSTRACT

In this paper, we study the printing of non-developable curved panels using existing 3D concrete printing technology combined with a novel Adaptable Membrane Formwork. The Adaptable Membrane Formwork consists of a grid of threaded rods, whose heights are adjustable and covered by a membrane sheet. Using this method, we were able to 3D-print, for the first time, Saddle and Dome-shaped concrete surfaces, which are non-developable. The printed specimens had good print quality and geometric fidelity, as shown by quantitative assessment. The proposed method thus demonstrates great potential for the 3D printing of freeform, curved and architectural facades.

© 2019 Elsevier Ltd. All rights reserved.

1. Introduction

Curvature adds possibilities to architecture that would not exist if only straight lines and linear layer surfaces make up the architect's toolbox. The use of curvature results in richer and more expressive designs. Although the use of curvature is not new, until now it has mainly been restricted to high profile projects or iconic architecture. This is caused by the higher costs of curved buildings as result of the extra effort needed for correct measurements in drawings and on the building site, the need for unconventional construction methods on the building site, or, in case of manufacturing, the extra costs of manufacturing complex shapes in the factory.

3D concrete printing has demonstrated its potential to disrupt the construction industry by printing concrete walls without conventional formworks [1]. 3D concrete printing achieves this by modifying the cementitious mix design to allow for higher fresh yield strength, fast setting and easy extrudability. This mix design is extruded from a nozzle that is accurately positioned with a

robotic/gantry printing system. The extruded cementitious mix is printed in a layer wise manner and the concrete structure is built up without formwork. This system is first described as Contour Crafting [2] and has been the basis for other 3D concrete printing setup [3]. In this generic printing setup, 3D Concrete printing has a limitation of not being able to fabricate overhung parts because of the cementitious material's low green strength properties after extrusion. Unless the cementitious material is reinforced or the use of corbeling (cantilevering) is used, significantly overhung parts cannot be printed [4]. As such, to print non-developable surfaces, it is necessary to provide temporary supports to print gradient and curved structures.

Other pioneers of 3D concrete printing have explored Shotcrete 3D Printing so as to print freeform 3D structure with large overhangs [5,6]. Lindemann et al. [5] describes Shotcrete 3D Printing as a highly controlled process using a robotic arm to spray the concrete onto a surface so as to build up the 3D structure. However Lindemann et al. also mentioned that due to the complexity involved in Shotcrete 3D printing, the resolution and accuracy of the printed 3D structure is difficult to achieve.

In this paper, we investigate a method to support the printing of doubly-curved concrete surfaces, which are non-developable, on

* Corresponding authors.

E-mail addresses: jianhui@ntu.edu.sg (J.H. Lim), ywweng@ntu.edu.sg (Y. Weng), cuong@ntu.edu.sg (Q.-C. Pham).

an Adaptable Membrane Formwork. The system is a temporary formwork consisting of a grid of adjustable threaded rods, covered by a flexible membrane. We used a specifically-designed algorithm to slice and generate the curved print path for 3D concrete printing. This experimental method is evaluated with regards to surface quality and geometric fidelity.

The remainder of this paper is organized as follows. In Section 2, we review existing manufacturing techniques for curved concrete. In Section 3, we present in detail the proposed curved concrete printing set up. In Section 4, we report the results of the modeling and accuracy and precision assessment. In Section 5, we conclude by discussing the limitation of our current system and the direction for future work.

2. Related work

While 3D printing in the general sense promises the possibility of free form fabrication, 3D concrete printing has largely been limited to the printing of planar structures. This is due to the low yield strength of early age concrete that has just been freshly extruded. This low yield strength prevents overhanging concrete from being printed, hence to date free standing free form curved concrete structures have not been printed.

The common strategy to manufacture curved concrete is to cast concrete using static formwork. To increase the efficiency and reusability of the system, reusable mould systems have been developed. Renzo Piano first introduced the idea of a flexible formwork for the production of freely formed panels in the 1960's, however it has proved difficult to manufacture double curved concrete panels in practices. PERI introduced a wall formwork system that uses pre-assembled panels for curved walls [7]. However, PERI's system is only suited for the construction of single curved elements, with a minimum radius of 1 m. ADAPA developed a flexible formwork that prefabricate non-structural double curved concrete facade panels [8]. The formwork consisted of a membrane that is supported and adjusted by CNC controlled actuators. The membrane is flexible enough to form double curved shapes and stiff enough to avoid sagging between the actuators under the load of the concrete. ADAPA's system requires the concrete to be first poured on to the planar shaped formwork prior to the actuators deforming the concrete into the defined double curved geometry, after the concrete has gained sufficient strength through curing. However ADAPA's system would thus risk discontinuities in the curing concrete and as it bends the concrete after the concrete has set. In a similar work by Schipper et al. [9], their group adopted the same technique as ADAPA and manufactured doubly curved concrete through deliberate deformation of the flexible mould after casting. In their work, they studied mainly the rheological properties of concrete, as they recognize that deliberate deformation of concrete in an open mould, can cause the concrete to either spilled out of the mould if the concrete has not cured sufficiently or cracked if the concrete is too stiff. In addition, the maximum radius of curvature achieved by their system is 1.5 m.

In 3D printing application, Costanzi et al. [10] discussed the possibility of adopting a flexible mould developed at TU Delft for 3D printing applications. In the paper, they highlighted a possible work flow of using a flexible mould alongside 3D concrete printing. However Costanzi et al. did not print the concrete over a flexible mould, instead they printed the perimeter of the structure over a CNC-milled static mould and cast concrete to fill the structure. Also, they did not provide a quantitative assessment of the print quality or of the geometric fidelity.

In this paper, we outlined the design, selection and simulation study for the Adaptable Membrane Formwork, open sourced algorithms to generate the printing path of curved structure and validation process for 3D printing of free formed curved structures. We will demonstrate 3D concrete printing of the full curved structure directly onto an Adaptable Membrane Formwork, in contrast to the work by Costanzi et al. This presents new challenges as unlike printing on a fully supported CNC-milled static mould, an adaptable mould would deform if the mould surface's force equilibrium is not accounted for. The force analysis is conducted in Abaqus to ensure that the Membrane formwork is not overly deformed that it loses geometrical consistency to the designed shape.

As the full curved structure is being printed using 3D printable concrete, as opposed to the work by Costanzi et al., there is the challenge of designing a printing path that produces smooth curved surfaces. In normal 3D concrete printing of curved structures, the curvature is digitalized. When combined with the stiff, shape retentive properties of 3D printable concrete, the printer produces a staircase effect (Fig. 1). This problem is not seen when casting concrete, as a self compacting concrete of good flowability can be used to allow the concrete to flow along the curve. However using self compacting concrete on a curved structure cannot guarantee that the produced curved surface is of uniform thickness. We adopted a method from curved layer fused deposition modeling in polymer 3D printing [11] to produce a smooth curved surface. Therefore, we expect our system to be able to produce surface with higher radius of curvature when compared to conventional printing of non rectilinear structure as described by Lim et al. [12].

3. Materials and methods

3.1. Adaptable membrane formwork

The Adaptable Membrane Formwork consists of a grid of threaded rods, whose heights are adjustable, covered by a membrane sheet. The rod grid and the membrane are further described below.

3.1.1. Rod grid

The rod grid is pictured in Fig. 2: it consists of 4×4 stainless steel threaded rods of 10 mm diameter and 300 mm length. The distance between the centers of two neighboring rods is 70 mm, yielding a base surface of 210 mm \times 210 mm. The heights of the rods above the surface can be manually adjusted according to the

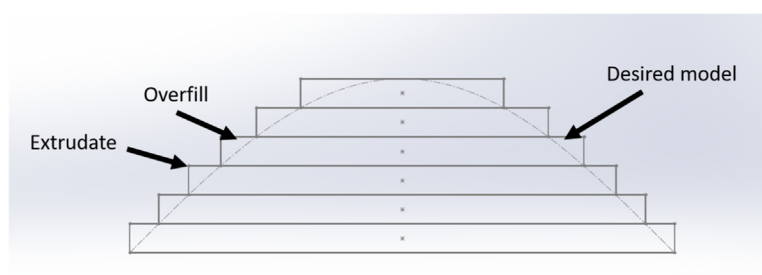


Fig. 1. Staircase effect in existing schemes for curved concrete printing.



Fig. 2. Rod grid with height-adjustable rods.

structure design, defining thereby a temporary surface on which the membrane formwork is laid. In the experiment, the individual rod heights are taken from the surface profile of the design structure and the rods rotated until the required height is reached. Alternatively, the rods could be fitted to servo motors, which would enable their heights to be automatically adjusted.

3.1.2. Printing structures

The doubly curved structures we set out to model and print are a Dome and a Saddle with base area of 210 mm×210 mm, mathematically defined by the following equations (see Fig. 5)

$$z_{\text{Dome}} = f_{\text{Dome}}(x, y) := (-\sqrt{(190^2 - x^2 - y^2)} + 190) \quad (1)$$

$$z_{\text{Saddle}} = f_{\text{Saddle}}(x, y) := \frac{\frac{x^2}{5} - \frac{y^2}{5}}{40} \quad (2)$$

3.1.3. Membrane selection

The membrane must be able to follow the curves and contours of the desired shape, without too much sagging. Fig. 3 shows two ways how a wrong membrane can affect the concrete panels: an overly rigid material prevents the membrane surface from being adjusted to the desired shapes, while an overly flexible material leads to uneven sagging on the surface. This sagging can be due to the weight of the cementitious material deforming the flexible membrane and causing it to lose its geometric fidelity, visually this can be observed as bumps on the printed panel.

As we are printing a non-developable surface, we require that the flexible formwork material to be sufficiently elastic, such that it may be stretched to the required dimension, and still sufficiently rigid to resist excessive deformation caused by the weight of the printed concrete, we estimated that Spandex (Young's modulus of 200 MPa and Poisson's ratio of 0.3) is a good option. To verify this hypothesis, we conducted a Finite Element Modeling (FEM) analysis in Abaqus, reproducing the actual loading conditions, rod spacing, etc. A linear elastic model was used in the FEM analysis for a light bidirectional woven flexible membrane of 2 mm thickness, undergoing uniform loading due to the weight of the

printed concrete. As the flexible member is expected to be reusable, it should not experience any plastic strain and is assumed that the deformation of the flexible membrane remains in the elastic region. The flexible membrane is meshed with a total of 44100 elements, with a mesh density of 1 mm.

We then compared the results of the FEM simulation to the desired shape. For completeness, we also conducted the FEM simulation for two other materials: Wood (Young's modulus of 15000 MPa and Poisson's ratio of 0.35) and Rubber (Young's modulus of 1 MPa and Poisson's ratio 0.5) and compared to the desired shape.

The membrane experiences increased loading with increasing number of concrete layer being printed on it. As such, to minimize loading, only one layer of concrete is printed on the membrane formwork. The thickness of the concrete layer can be increased by increasing the nozzle stand off distance from the membrane formwork and increasing the diameter of the extruder nozzle. If multiple layers of the concrete panel is required to be printed, the concrete is allowed to cured and gain enough yield strength before subsequently layers are printed on it. This would allow the concrete panel to bear the additional load, and avoid causing additional strain on the membrane formwork. However the subsequent layers should be printed while the prior layer is still fresh, as the bond strength at the interface degrades if the time gap between printing exceeds the printability time.

The results from the FEM simulation of the three materials are intersected with 6 test planes normal to $x = -60$ mm, 0 mm, 60 mm and $y = -60$ mm, 0 mm, 60 mm. These planes were chosen so as to lay in-between the support nodes and thus likely to contain the greatest Z-errors ϵ , due to sagging or bulging of the membrane.

Next, we evaluate the print quality as follows. For each point $(x_{\text{FEM}}, y_{\text{FEM}}, z_{\text{FEM}})$ of the FEM simulation, the Z-errors ϵ between the model defined by Eqs. (2) and (1) and the results of the FEM are given by

$$\epsilon_{\text{Saddle}} := |z_{\text{FEM}} - f_{\text{Saddle}}(x_{\text{FEM}}, y_{\text{FEM}})|,$$

and similarly for ϵ_{Dome} .

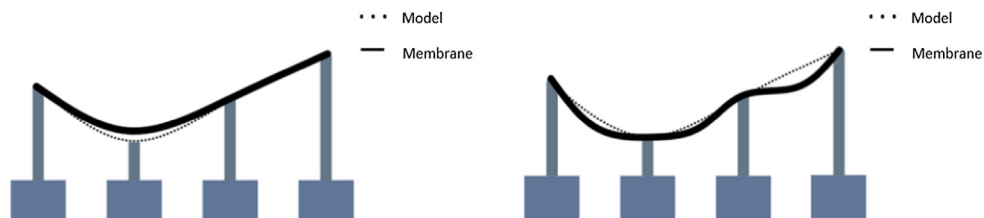


Fig. 3. Effect of the flexibility of the membrane material. Left: high Young's modulus (stiff). Right: low Young's modulus (flexible).

For each test plane \mathcal{P} , we select all the points $(x_{\text{FEM}}, y_{\text{FEM}}, z_{\text{FEM}})$ located within a distance of 0.5 mm from \mathcal{P} , and compute the mean and standard deviation of the Z-errors ϵ across those points.

3.2. Printing system

Fig. 4 shows the physical printing setup, which comprises a 6-axis robotic arm, a concrete mixing and delivery system (mixer, pump, hose, nozzle), and the Adaptable Membrane Formwork. The robot is mounted on a mobile platform, which could allow the printing system to print larger structures [13,14].

The robotic arm has a horizontal reach of 87 cm with an accuracy and repeatability of 0.02 mm. The accuracy and repeatability of the robotic arm is a measure of the performance of the robotic arm. The robotic arm can repeatedly achieve precise positioning of the end effector when executing the same task, this makes it highly suitable for positioning the extruder nozzle of a 3D concrete printing system. A extruder nozzle is mounted to the end effector of the arm, and a hose pipe attached around the length of the arm. The pump system delivers cementitious material to the extruder nozzle for selective deposition of concrete. The printing path can be generated from a given design or CAD file and sliced into a series of tool path coordinates for the robotic extruder nozzle to follow, and build up the printed structure. Our path planning system will solve for feasible and reasonable pose for each tool coordinate [13,14]. A feasible solution is defined if the robotic arm can position the extruder nozzle accurately onto the printing path without self collision or exceeding its joint limit. While a reasonable solution is defined if the robotic arm is able to avoid failure points if there is a better solution.

3.3. Printing materials and process

Formulations used in this study consist of Ordinary Portland Cement (OPC, ASTM type I, Grade 42.5) [15], silica fume (SF, Undensified, Grade 940, Elkem company) [16], river sand, fly ash

(FA, Class F) [17], natural river sand, water and superplasticizer (SP). The mix design of the concrete is important to maintain good extrudability and shape stability of the concrete filament. Mixing process is fixed to maintain rheological consistence [18]. After printing, the concrete shell structure is covered by a plastic sheet and demolded after one day [19] (Table 1).

3.4. Generation of printing path

Using the equations of the Dome and Saddle in (2) and (1), one can generate PLY files, which are then processed as point clouds. The point clouds are digitally orientated onto the membrane formwork. The points and normals were taken from the bottom surface of the point cloud using a normal estimation algorithm.

The points and their normals of the point clouds were arranged in according to a print path strategy that starts from the lowest point to the highest point without overlaying of the path as shown in **Fig. 5**. The print path starts from blue to red. This print path strategy allows for fresh concrete to be printed on the prevailing concrete filament and hence a more stable built up of filaments. The print path is also designed to be continuous to avoid disruption and throttling of the concrete extruder pump. This ensures that the concrete undergoes a constant flow rate and will not disturb the rheological properties of the concrete caused by changes in the shear rate of the extruder pump.

3.5. Print validation method

As the technique of printing doubly curved concrete structure is targeted at printing architectural designed structures, the concrete panel is measured for geometrical fidelity and aesthetics. Given that the concrete panel is doubly curved, and to be able to capture all the measurement in its entirety, we chose imaging techniques as our validation method. In a previous paper, researchers have used a Kinect V2 3D camera to help map out the surface shape of a fresh concrete cylinder as it undergoes deformation [20].

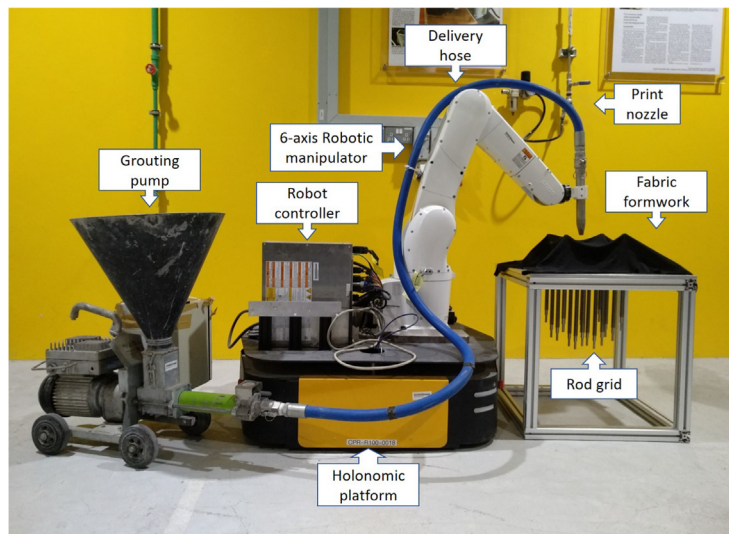
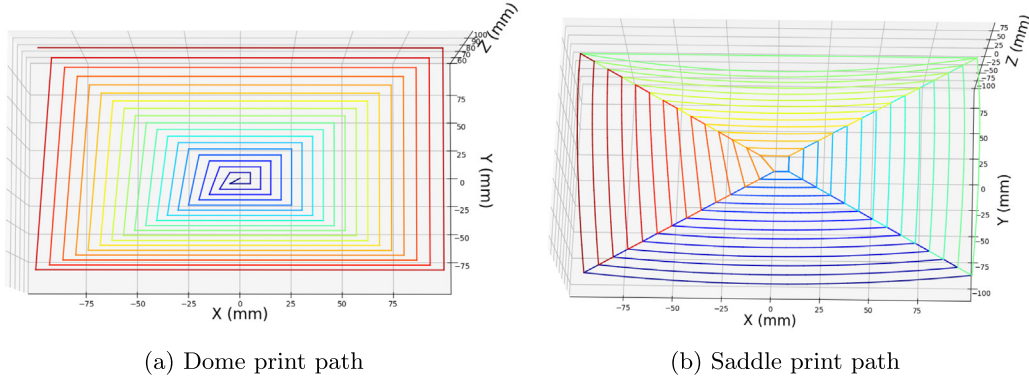


Fig. 4. Experimental setup comprising robotic printing system and Adaptable Membrane Formwork.

Table 1
Mixture proportions.

Materials	OPC	Sand	Water	Fly ash	Silica fume	Superplasticizer/(g/l)	PVA fibre
Proportion	1	0.5	0.3	1	0.1	1.3	0.05

Note: All ingredients contents are expressed as weight proportion of cement content.

**Fig. 5.** Printing path.

The printed structure is placed against a clear background, at a distance of 0.5 m normal to a Kinect V2 3D camera. The printed structure is ensured to be free from occlusion, and the bottom surface can be captured. The captured point cloud is then registered to the model point cloud using an iterative closest point (ICP) algorithm [21], and compared for Z-errors ϵ .

The ICP algorithm is able to handle the 6 degrees of freedom and perform rigid transformation of the captured point cloud, until the mean-square distance metric of the points in the captured point cloud is minimized against the points in the model point cloud. As the ICP algorithm described in [21] is known to converge monotonically to the nearest local minimum of the mean-square distance metric, a good initial alignment and pre-processing is required.

The captured point cloud is first pre-processed by passing through a pass-through filter that removes points in the background and NaN points. This step would effectively segment the points of the printed structure from the captured point cloud. Subsequently, a statistical outlier removal filter is also used to remove all noises from the capture point cloud. The initial alignment of the captured point cloud of the printed structure is transformed manually by objectively positioning the printed structure in the same normal direction as the model

point cloud. The ICP algorithm is then applied to refine the pose of the point cloud.

The refined point cloud is then intersected with 6 test planes normal to $x = -60 \text{ mm}, 0 \text{ mm}, 60 \text{ mm}$ and $y = -60 \text{ mm}, 0 \text{ mm}, 60 \text{ mm}$. These planes were chosen so as to lay in-between the support nodes and thus likely to contain the greatest Z-errors ϵ .

Next, we evaluate the print quality as follows. For each point $(x_{\text{printed}}, y_{\text{printed}}, z_{\text{printed}})$ of the point cloud, the Z-errors ϵ between the model defined by Eqs. (2) and (1) and the printed specimen are given by

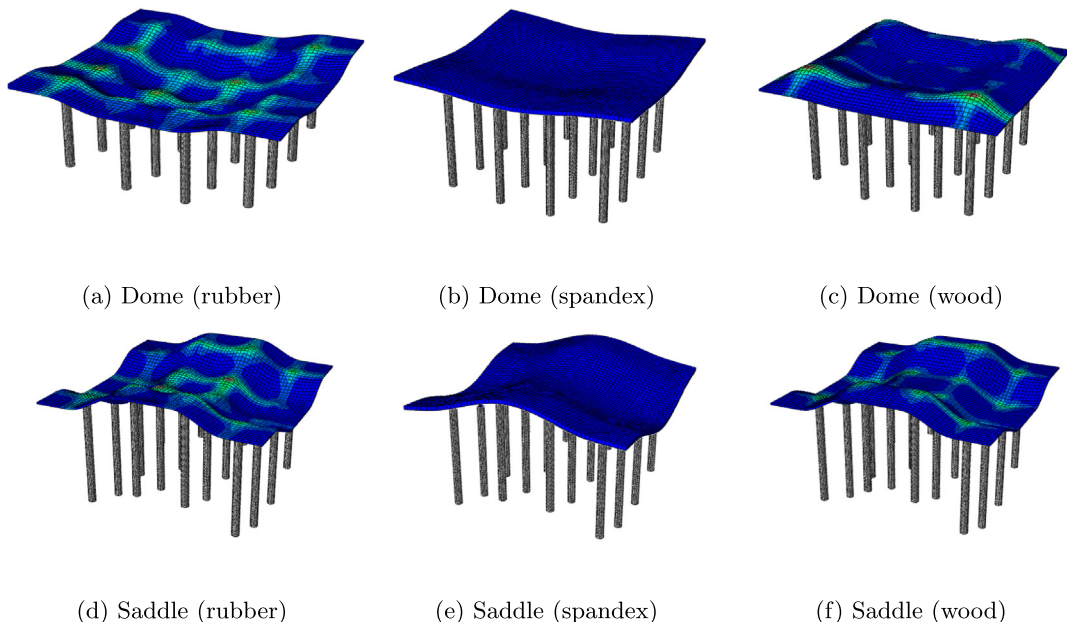
$$\epsilon_{\text{Saddle}} := |z_{\text{printed}} - f_{\text{Saddle}}(x_{\text{printed}}, y_{\text{printed}})|,$$

and similarly for ϵ_{Dome} .

For each test plane \mathcal{P} , we select all the points $(x_{\text{printed}}, y_{\text{printed}}, z_{\text{printed}})$ located within a distance of 0.5 mm from \mathcal{P} , and compute the mean and standard deviation of the Z-errors ϵ across those points.

4. Results

Results of both simulation on selection of membrane and printing of concrete shell structures are presented in this section.

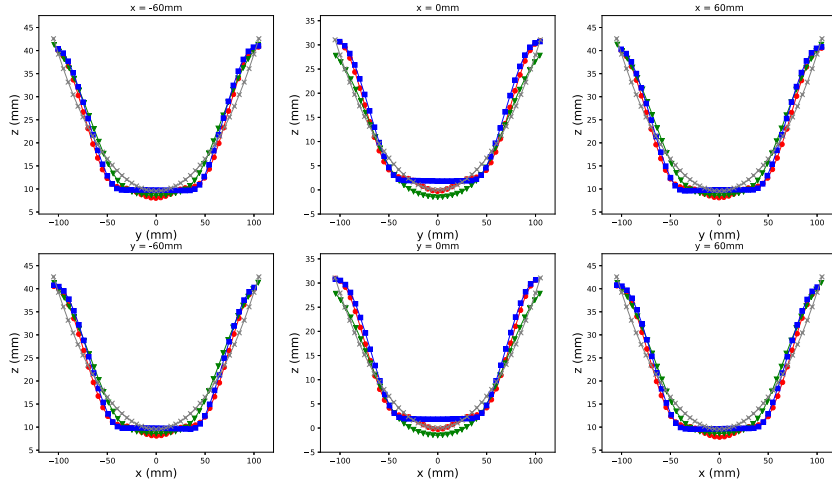
**Fig. 6.** Comparison of the Dome model and the Saddle model using different materials in FEM.

4.1. Membrane modeling

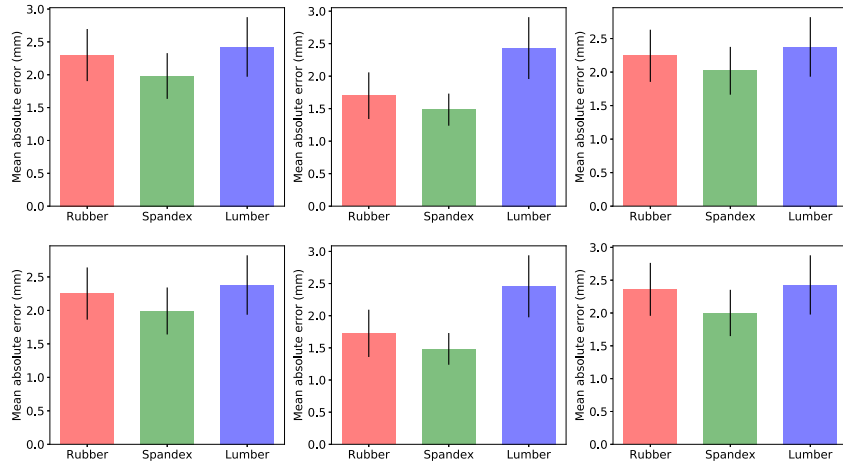
Fig. 6 shows the FEM model of the 3 different materials for the Dome and Saddle structure. In **Fig. 6(a), (d)**, for model built using the rubber, there is noticeable sagging of the surface when under loading due to the weight of the concrete deposited when printing. While in **Fig. 6(c) and (f)**, the center of the surface retains a distinct

planar face as it resists the bending forces from the weight of the concrete. It is only in **Fig. 6(b)** and **(e)**, that the surface is still curved after concrete printing.

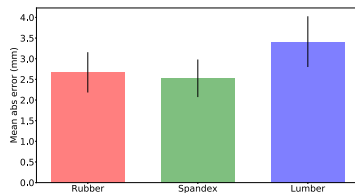
As such, it can be seen that it is necessary to carefully select the right material that is sufficiently flexible to be bend into shape and stiff enough to resist sagging when concrete is printed over it.



(a) Surface profile of the 3 materials at $[x = -60\text{ mm}, 0\text{ mm}, 60\text{ mm}$ and $y = -60\text{ mm}, 0\text{ mm}, 60\text{ mm}.]$



(b) Mean absolute Z-errors ϵ of the 3 material at $[x = -60\text{ mm}, 0\text{ mm}, 60\text{ mm}$ and $y = -60\text{ mm}, 0\text{ mm}, 60\text{ mm}.]$

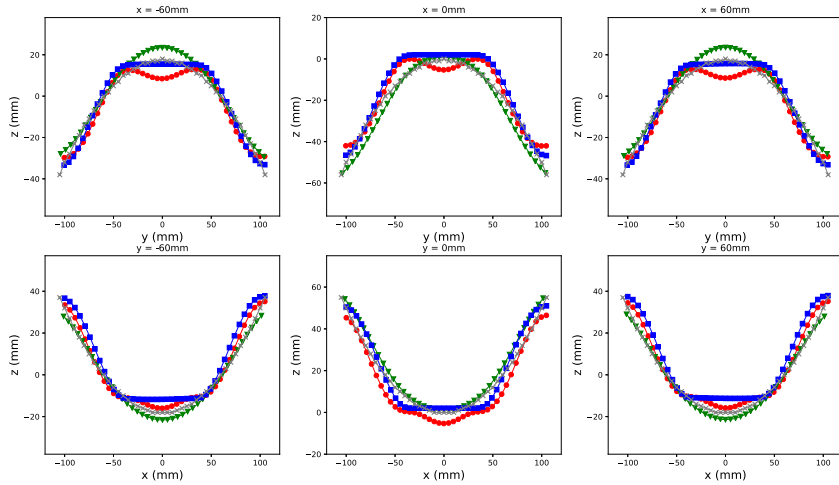


(c) Mean absolute Z-errors ϵ over the full surface

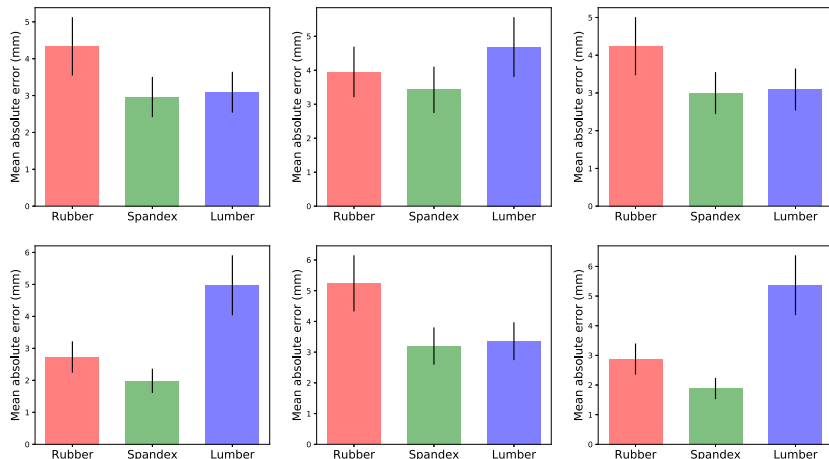
Fig. 7. Comparison of the Dome model and the different surface at 3 planes simulated by Finite Elements.

Fig. 7 and **Fig. 8** shows the comparison of the different materials against the desired model at 6 test planes normal to $x = -60$ mm, 0 mm, 60 mm and $y = -60$ mm, 0 mm, 60 mm. **Fig. 7a** and **Fig. 8a** shows the surface profile of the different materials against the desired model. **Fig. 7b** and **Fig. 8b** shows the mean absolute Z-errors ϵ of the different materials and the standard deviation of the Z-errors ϵ over the 6 test planes.

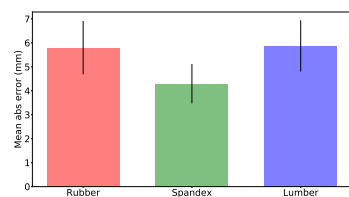
It is observed that the profiles of the spandex material follows the closest to the model profile, with a mean absolute error of 2.5 mm, standard deviation of 0.45 mm and mean absolute error of 4 mm and standard deviation of 0.8 mm for the dome and saddle shape respectively. This is in comparison to the rubber with mean absolute error of 2.7 mm and 5.8 mm and the lumber with mean absolute error of 3.4 mm and 5.9 mm for the dome and saddle shape.



(a) Surface profile of the 3 materials at [$x = -60$ mm, 0 mm, 60 mm and $y = -60$ mm, 0 mm, 60 mm.]



(b) Mean absolute Z-errors ϵ of the 3 material at [$x = -60$ mm, 0 mm, 60 mm and $y = -60$ mm, 0 mm, 60 mm.]



(c) Mean absolute Z-errors ϵ over the full surface

Fig. 8. Comparison of the Saddle model and the different surface simulated by Finite Elements.

Additionally, the rubber model shows significant sagging in the saddle model, with the weight of the concrete depressing the rubber membrane. The lumber model shows significant resistance to bending in both the dome and saddle model, as its young modulus is too high and it does not deform to fit the model. This results in higher mean absolute error for both rubber model and lumber model.

The flexible mould assumes the geometry of the designed shape and must have sufficient strength required to resist bending and the loading from the concrete printing while maintain geometrical fidelity.

The finite element model shows good agreement with the CAD model with mean absolute error less than 4 mm for both the Dome and Saddle structure. This demonstrate that the selected material

(spandex) is capable of bearing the pressure exerted by the fresh concrete and the bending required to adhere to the curvature of the CAD model, at a rod spacing of 70 mm, in a 4×4 grid setup.

The finite element model shows localized stress, particularly in the area where the rods are. Those areas have a higher stress state than other regions and may be areas where higher strain is likely to occur at this localized area.

4.2. Printed structures

The printed shell structures are shown in Fig. 9. The structures is visually smooth, with no observable surface roughness, as it was printed with mortar grade cementitious mixture using fine



Fig. 9. Printed structures, viewed from the top and from the bottom. Left: Saddle. Right: Dome.

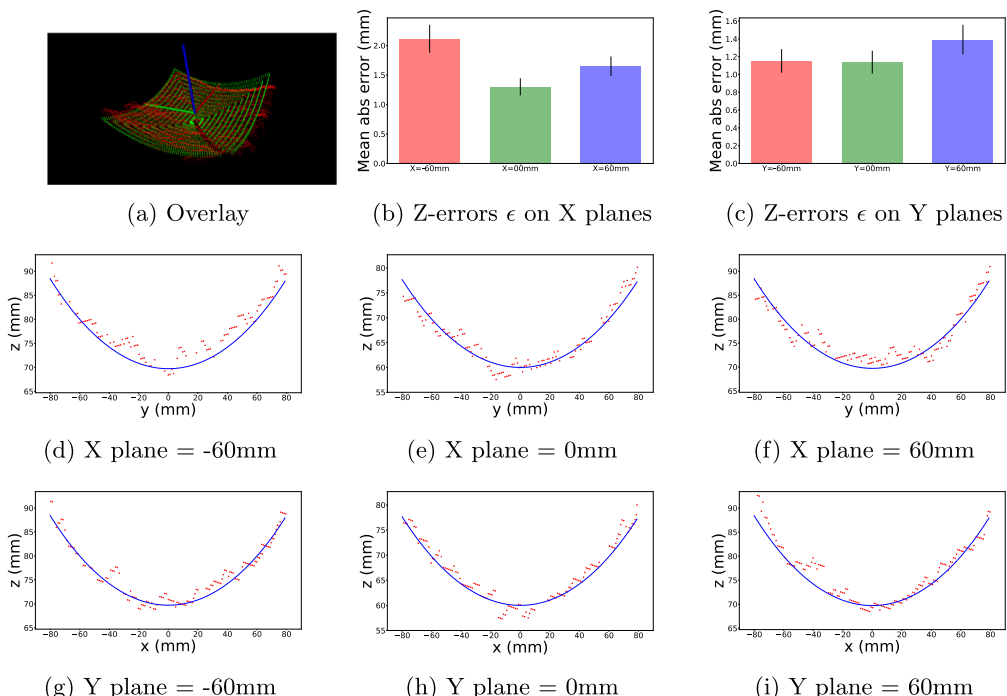


Fig. 10. Comparison of the Dome model and the actual printed surface measured by Kinect.

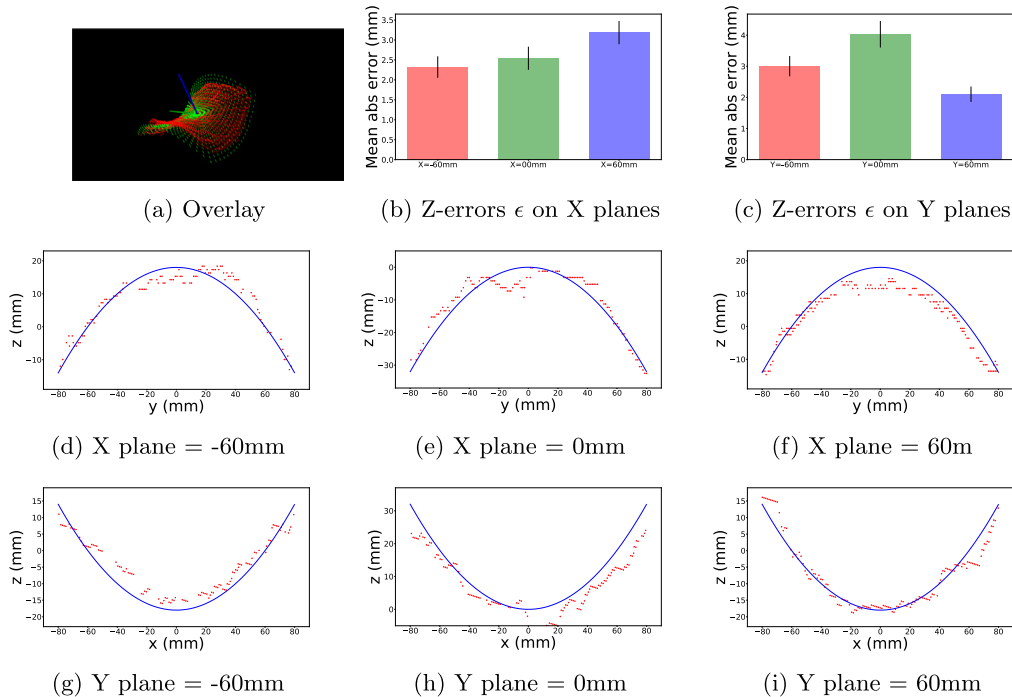


Fig. 11. Comparison of the Saddle model and the actual printed surface measured by Kinect.

aggregates. There is even color variation as the printing was done continuously using a single batch of cementitious mixture. There is no staircase effect between layers as the printing path is printed normal to the curved surface, rather than normal to the substrate print bed as in the generic 3D concrete printing setup. Using a vernier caliper and measuring along the edges, the shell thickness is roughly 10 mm.

4.3. Quantitative assessment of print quality

An overlay of the printed part's point cloud and desired model's point cloud is shown in the top right of Figs. 10 and 11.

Figs. 10(b), (c) and 11(b), (c) shows the distribution of Z-errors ϵ of the Dome shaped part and the Saddle shaped part against an imaginary plane that intersects the printed part normal to $x = -60$ mm, 0 mm, 60 mm and $y = -60$ mm, 0 mm, 60 mm. Individual plots of the profile of the printed parts against designed model can be found in Figs. 10d to i and 11d to i. It is observed that the profiles of the printed part are generally close to the target surface, with mean absolute error across the 6 planes is less than 2 mm for the dome, mean absolute error of 4 mm for the saddle. The biggest standard deviation is 0.5 mm from the mean absolute error. The maximum absolute error for the dome model and 9 mm for the saddle model.

The high standard deviation error might be attributed to the use of the Kinect V2 camera used to capture the point cloud. Yang et al. found that at a distance of 0.5 m, the average depth accuracy of the Kinect V2 camera is around 2 mm [22].

The robotic printer shows no bias in printing along the longitudinal direction or transverse direction. It is observed that the robotic printer shows a higher average absolute error of 4 mm when printing the Saddle part as compared to 2 mm when printing the Dome part. The maximum error observed is 5 mm on the dome and 9 mm on the saddle structure. As when printing the Saddle part, it is a hyperbolic paraboloid shape which would require more support nodes to accurately reflect its shape as compared to the Dome part.

When printing the Saddle part, which has a hyperbolic paraboloid shape, the printing path translates down along the x-axis and

up along the y-axis. This changing of gradient of the print path when simultaneously depositing concrete may have caused the printer to deposit an excess of concrete at those points, hence there are Z-errors of both positive and negative nature.

As all prints were performed on a thin spandex membrane, the actuators tips were seen to impart an indentation mark on the final product. We used a vernier caliper and measured along the edges of the printed part. The average shell thickness is found to be 10 mm.

5. Conclusion

This paper presents a novel method for the 3D-printing of curved concrete structures. Our setup consists of a 6-axis robotic printer and an Adaptable Membrane Formwork. This affords an increase in the level of flexibility and geometry complexity for the manufacturing process of concrete architectural elements. As a case study, we printed two non-developable, doubly-curved, surfaces: a Saddle and a hemisphere Dome. We showed that our setup could 3D-print these thin (10 mm) concrete shell elements with good accuracy and surface finishing. This opens the way to flexible yet economically-sustainable schemes for manufacturing curved concrete surfaces.

Declaration of Competing Interest

The authors declare that they have no known competing financial interests or personal relationships that could have appeared to influence the work reported in this paper.

Acknowledgements

This research was supported by the National Research Foundation, Prime Minister's Office, Singapore under its Medium-Sized Centre funding scheme, Singapore Centre for 3D Printing, and Sembcorp Design & Construction Pte Ltd. We would like to thank C. Soderberg, D. Quirin for helpful discussions, and Zhang Xu for helping with the experiment and with the manuscript.

References

- [1] J.G. Sanjayan, B. Nematollahi, 3d concrete printing for construction applications, in: 3D Concrete Printing Technology, Elsevier, 2019, pp. 1–11.
- [2] B. Khoshnevis, Automated construction by contour crafting-related robotics and information technologies, *Autom. Constr.* 13 (1) (2004) 5–19.
- [3] B. Nematollahi, M. Xia, J. Sanjayan, Current progress of 3d concrete printing technologies, ISARC. Proceedings of the International Symposium on Automation and Robotics in Construction, vol. 34, Gediminas Technical University, Department of Construction Economics, Vilnius, 2017, p. 34.
- [4] R.A. Buswell, W.L. de Silva, S. Jones, J. Dirrenberger, 3d printing using concrete extrusion: a roadmap for research, *Cem. Concr. Res.* 112 (2018) 37–49.
- [5] H. Lindemann, R. Gerbers, S. Ibrahim, F. Dietrich, E. Herrmann, K. Dröder, A. Raatz, H. Kloft, Development of a shotcrete 3d-printing (sc3dp) technology for additive manufacturing of reinforced freeform concrete structures, in: RILEM International Conference on Concrete and Digital Fabrication, Springer, 2018, pp. 287–298.
- [6] H. Lindemann, A. Fromm, J. Ott, H. Kloft, Digital prefabrication of freeform concrete elements using shotcrete technology, *Proceedings of IASS Annual Symposia*, vol. 2017, International Association for Shell and Spatial Structures (IASS), 2017, pp. 1–8, no. 6.
- [7] Peri, Rundflex circular wall formwork, accessed: 2018-11-30. [Online]. Available:<https://www.peri.com/en/products/formwork/wall-formwork/rundflex-circular-wall-formwork.html>.
- [8] C. Raun, P.H. Kirkegaard, Reconfigurable double-curved mould, in: Proceedings of the Second International Conference on Flexible Formwork: Full Papers. BRE CICM, University of Bath, 2012, pp. 292–299.
- [9] H. Schipper, S. Grünwald, P. Raghunath, Rheological parameters used for deliberate deformation of a flexible mould after casting, in: Proceedings of 7th RILEM International Conference on Self-Compacting Concrete and 1st RILEM International Conference on Rheology and Processing of Construction Materials, 2013.
- [10] C.B. Costanzi, Z. Ahmed, H. Schipper, F. Bos, U. Knaack, R. Wolfs, 3d printing concrete on temporary surfaces: the design and fabrication of a concrete shell structure, *Autom. Constr.* 94 (2018) 395–404.
- [11] O. Diegel, S. Singamneni, B. Huang, I. Gibson, Curved layer fused deposition modeling in conductive polymer additive manufacturing, *Advanced Materials Research*, vol. 199, Trans Tech Publ, 2011, pp. 1984–1987.
- [12] S. Lim, R.A. Buswell, T.T. Le, R. Wackrow, S.A. Austin, A.G. Gibb, T. Thorpe, Development of a viable concrete printing process, 2011..
- [13] X. Zhang, M. Li, J.H. Lim, Y. Weng, Y.W.D. Tay, H. Pham, Q.-C. Pham, Large-scale 3d printing by a team of mobile robots, *Autom. Constr.* 95 (2018) 98–106.
- [14] M.E. Tiryaki, X. Zhang, and Q.-C. Pham, Printing-while-moving: a new paradigm for large-scale robotic 3d printing, arXiv preprint arXiv:1809.07940, 2018..
- [15] A.S.C. C.-A, Standard specification for portland cement, West Conshohocken, PA: ASTM International, 2019.<http://www.astm.org>.
- [16] A.S.C., Standard specification for silica fume used in cementitious mixtures, West Conshohocken, PA: ASTM International, 2019,<http://www.astm.org>.
- [17] A.S.C., Standard specification for coal fly ash and raw or calcined natural pozzolan for use in concrete, West Conshohocken, PA: ASTM International, 2019,<http://www.astm.org>.
- [18] B. Zareian, B. Khoshnevis, Effects of mixture ingredients on extrudability of concrete in contour crafting, *Rapid Prototyping J.* 24 (4) (2018) 722–730.
- [19] Y. Weng, B. Lu, M.J. Tan, S. Qian, Rheology and printability of engineered cementitious composites-a literature review, in: Proceedings of the 2nd International Conference on Progress in Additive Manufacturing (Pro-AM 2016), Research Publishing, Singapore, 2016, pp. 427–432.
- [20] B. Panda, J.H. Lim, M.J. Tan, Mechanical properties and deformation behaviour of early age concrete in the context of digital construction, *Compos. Part B: Eng.* 165 (2019) 563–571.
- [21] P.J. Besl, N.D. McKay, Method for registration of 3-d shapes, *Sensor Fusion IV: Control Paradigms and Data Structures*, vol. 1611, International Society for Optics and Photonics, 1992, pp. 586–607.
- [22] L. Yang, L. Zhang, H. Dong, A. Alelaiwi, A. El Saddik, Evaluating and improving the depth accuracy of kinect for windows v2, *IEEE Sens. J.* 15 (8) (2015) 4275–4285.